



Amelioration of White Matter Injury Through Mitigating Ferroptosis Following Hepcidin Treatment After Spinal Cord Injury

Jiantao Shi¹ · Xingsen Xue¹ · Linbo Yuan¹ · Guangjian He¹ · Zhouyang Jiang¹ · Long Wang¹ · Jiali Zhang¹ · Hong Su¹ · Jishu Xian¹ · Chuhua Fu^{1,2} · Shengli Hu¹

Received: 29 October 2022 / Accepted: 1 February 2023 / Published online: 28 February 2023
© The Author(s), under exclusive licence to Springer Science+Business Media, LLC, part of Springer Nature 2023

Abstract

Spinal cord injury (SCI) usually introduces permanent or long-lasting neurological impairments. Maintaining the integrity of the limited number of white matter bundles (5–10%) preserves wholly or partially locomotor following SCI. Considering that the basic structure of white matter bundles is axon wrapped by oligodendrocytes, promoting oligodendrocytes survival might be a feasible strategy for reducing white matter injury (WMI) after SCI. Oligodendrocytes are rich in unsaturated fatty acid and susceptible to ferroptosis-induced damage. Hence, exploring method to reduce ferroptosis is supposed to expedite oligodendrocytes survival, thereafter mitigating WMI to facilitate functional recovery post-SCI. Here, the results indicated the administration of hepcidin reduced iron accumulation to promote oligodendrocytes survival and to decrease spinal cord atrophy, therefore facilitating functional recovery. Then, the WMI was evidently decreased owing to attenuating ferroptosis. Subsequently, the results revealed that the expression of divalent metal transporter 1 (DMT1) and transferrin receptor (TfR) was expressed in CC1⁺ cells. The expression level of DMT1 and TfR was significantly increased, while this phenomenon was obviously neutralized with the administration of hepcidin in the epicenter of spinal cord after SCI. Afterward, the application of hepcidin downregulated reactive oxygen species (ROS) overload, which was evidently increased with the treatment of 20 μM FeCl₃, therefore increasing cell viability and reducing lactate dehydrogenase (LDH) activity through downregulating the expression of DMT1 and TfR to inhibit ferroptosis in oligodendrocyte progenitor cells (OPCs). The present study provides evidence that the application of hepcidin facilitates oligodendrocytes survival to alleviate WMI via reducing the expression of DMT1 and TfR.

Keywords Spinal cord injury · Hepcidin · Ferroptosis · White matter injury · Reactive oxygen species

Abbreviations

SCI Spinal cord injury
WMI White matter injury
DMT1 Divalent metal transporter 1

TfR Transferrin receptor
ROS Reactive oxygen species
LDH Lactate dehydrogenase
OPCs Oligodendrocyte progenitor cells
GPER1 G-protein coupled estrogen receptor 1
NSC Neural stem cell
MSC Mesenchymal stem cell
Fpn1 Ferroportin 1
PBS Phosphate-buffered saline
DMEM Dulbecco's modified Eagle's medium
bFGF Basic fibroblast growth factor
PDGF Platelet-derived growth factor
HE Hematoxylin and eosin
IHC Immunohistochemistry
DAB 3-Diaminobenzidine
TEM Transmission electron microscopy
BCA Bicinchoninic acid
PVDF Polyvinylidene difluoride

Jiantao Shi, Xingsen Xue and Linbo Yuan contributed equally to this work.

✉ Chuhua Fu
nianbeifch@163.com

✉ Shengli Hu
husl1937@163.com

¹ Department of Neurosurgery and Key Laboratory of Neurotrauma, Southwest Hospital, Third Military Medical University (Army Medical University), 400038 Chongqing, People's Republic of China

² Department of Neurosurgery, Xiangyang No.1 People's Hospital, Hubei University of Medicine, 441011 Xiangyang, Hubei, People's Republic of China

CCK8	Cell counting kit-8
dMBP	Degraded myelin basic protein
APP	Amyloid precursor protein
AD	Alzheimer's disease
HRP	Horseradish peroxidase
RT-qPCR	Reverse transcription-quantitative polymerase chain reaction
FSP1	Ferroptosis suppressor protein 1 (FSP1)

Introduction

Spinal cord injury (SCI), a devastating disorder with serious neurological deficits and a small chance of recovery, usually introduces permanent or long-lasting neurological impairments [1, 2]. The pathology of neurological deficits ascribes to primary and secondary injury. The effective therapy for primary injury is surgery, while the mechanism of secondary injury is complicated. Therefore, targeting secondary injury is a feasible regimen for improving neurological deficits after SCI. Our previous studies have found out a series of therapeutic candidates targeting secondary damage, including reducing glial scar formation and enhancing axon rehabilitation through the administration of curcumin, anti-sense vimentin cDNA combined with chondroitinase ABC [3–5], decreasing neuronal loss by blocking acid-sensing ion channel 1a (ASIC 1a) [6] or activating G-protein coupled estrogen receptor 1 (GPER1) [7, 8], and suppressing complement C5a [9]. Cell replacement therapy including promoting endogenous neural stem cell (NSC) differentiation into neurons [10, 11] and the transplantation of human umbilical cord mesenchymal stem cell (MSC) [12] shows some beneficial performance in SCI model. However, the therapeutic effect is still far from ideal, suggesting that more mechanisms related to secondary injury need to be elucidated.

Our previous studies have mainly focused on the research of neuronal damage, survival and regeneration of neurons. However, recent studies have indicated that maintaining the integrity of limited number of white matter bundles (5–10%) could preserve wholly or partially locomotor during the acute and/or chronic stage of SCI [13–15]. Given that the basic structure of white matter bundles is axon wrapped by oligodendrocytes, promoting oligodendrocytes survival is a feasible strategy for preserving the integrity of white matter bundles to reduce white matter injury (WMI) after SCI. Oligodendrocytes, the main neural subtype responsible for surrounding axons in the central nervous system (CNS), are rich in unsaturated fatty acid [4] and susceptible to ferroptosis-induced damage [16]. Ferroptosis, a form of nonapoptotic form of cell death, is characterized by iron-dependent lipid peroxidation, and ferroptotic cells exhibit shrunken mitochondria, smaller mitochondrial area, and

increased membrane density [17, 18]. Previous studies have demonstrated ferroptosis is a common pathology resulting from iron and reactive oxygen species (ROS) overload in the epicenter of spinal cord following SCI [17, 19, 20]. Herein, exploring method to reduce ferroptosis is supposed to expedite oligodendrocytes survival, thereafter mitigating WMI to facilitate functional recovery post-SCI.

Hepcidin is a secreted peptide hormone encoded by the hepcidin antimicrobial peptide (HAMP) gene and generated mainly by the liver [21]. Increased hepcidin expression decreases iron content by binding with ferroportin 1 (Fpn1), and then blocks iron export from hepatocytes, enterocytes, cardiomyocytes, and macrophages [21–23]. The administration of hepcidin peptide evidently downregulates the expression of cell-iron-uptake proteins including transferrin receptor (TfR) and divalent metal transporter 1 (DMT1), thereafter reducing iron release in cultured microvascular endothelial cells [24]. Furthermore, hepcidin holds the capacity of reducing iron uptake and release in cultured astrocytes and neurons through decreasing the expression of Fpn1, TfR and DMT1 [24, 25], suggesting that the application of hepcidin might downregulate TfR and DMT1 to alleviate oligodendrocytes injury after SCI. However, the effect of hepcidin on reducing WMI and the underlying mechanism remain elusive.

In the present study, we posited that oligodendrocytes ferroptosis induced by iron and ROS overload played an important role in WMI after SCI, and the application of hepcidin mitigated oligodendrocytes ferroptosis via reducing iron and ROS accumulation through downregulating the expression of TfR and DMT1, thereafter reducing WMI to promote functional recovery post-SCI. The aim of the present study is to certify the therapeutic effect of hepcidin on SCI in rats, and to offer a possible therapeutic strategy for SCI, even for other CNS diseases existing ferroptosis, from bench to bedside.

Materials and Methods

Animals

The animal experiment procedures were implemented according to the China's animal welfare legislation for the protection of animals used for scientific purposes. And, this work was supervised by the Ethics Committee of the Southwest Hospital, Third Military Medical University (Army Medical University) for the use of laboratory animals (approval no. AMUWEC20210017). A total of 20 P0–P1 Wistar rats and 77 adult female (200–250 g, 10–12 weeks, 69 rats used for experiments and 8 rats died during experiments) Wistar rats were used for establishing SCI model in the present study. All rats were housed in a constant

condition (12-h light/dark cycle, 22–25 °C, 55–60% moisture) and given free access to food and water before and after surgery.

The Establishment of Rat SCI Model

The rat SCI model was established as previously described [1, 26]. Briefly, a stereotaxic frame was applied to fixed the rats after they were anaesthetized with 2% isoflurane/air mixture (2–3 l/min). Then, a 4-cm-long skin incision was made in the midline of the back over the spinal cord, and the thoracic 9–11 (T9–11) spinal segments was exposed by performing a laminectomy, leaving the dura intact. Afterward, spinal contusion was implemented using a 20-g weight rod (diameter 4 mm) dropping from a height of 30 mm onto the exposed T10 segment. Subsequently, the muscles, subcutaneous tissue, and skin were separately sutured. During surgery, rat body temperature was maintained at 37 ± 0.3 °C using a feedback-controlled heating pad system (Zhongshi, Inc., Beijing, China). After surgery, rats were received manual bladder empty twice a day until they could do themselves, even appropriate veterinary care if needed. The dehydration, weight loss, autophagia, and discomfort were recorded per day.

Experimental Groups

After surgery, rats were randomly divided into the following groups using the random number table method:

- (i) Sham group. Rats, received laminectomy without contusion, were intra-spinally microinjected the same volume of 0.01 M phosphate-buffered saline (PBS, pH 7.4), equivalent to the volume of hepcidin solution in SCI+hepcidin group, using the same method.
- (ii) SCI group. Rats, received laminectomy with contusion, were intra-spinally microinjected the same volume 0.01 M PBS (pH 7.4), equivalent to the volume of hepcidin solution in SCI+hepcidin group, using the same method.
- (iii) SCI+hepcidin group. Rats, received laminectomy with contusion, were intra-spinally microinjected recombinant mouse hepcidin (cat no. RPB979Mu01, 0.7 mg/kg, Cloud-Clone Corp., Katy, TX, USA) 4 h after surgery. Hepcidin was diluted in 0.01 M PBS (pH 7.4) and microinjected into the dorsal spinal cord 2 mm rostrally and 2 mm caudally to the injury site at a depth of 1.2 mm and 0.75 mm laterally from midline at a rate of 1 μ l/min. Afterward, the needle was left in position for a 2 min before being slowly withdrawn. A total volume of 10 μ l hepcidin was injected. The second dosage was performed on the second day after SCI.

The BBB Locomotor Rating Score

The Basso, Beattie, and Bresnahan (BBB) locomotor rating score is a 21-point scale that is universally applied to determine the behavioral outcomes after SCI in rats [27]. The rating score ranges from 0 to 21: 0 exhibits no locomotor function and 21 shows normal performance. In short, rats were placed in a 90-cm² field and allowed them to walk around freely for 5 min, and the movements of hind limb were closely observed and recorded using a camera. Subsequently, the BBB locomotor rating score was assessed by two independent examiners blinded to the experimental groups on days 7, 35, and 56.

Primary OPC Culture

Primary oligodendrocyte progenitor cells (OPCs) were isolated from P0–P1 Wistar rats as previously described [1]. In brief, the spinal cord tissues were dissected under a stereomicroscope (SZ61, Olympus, Tokyo, Japan) after the dura mater and blood vessels were removed. Thereafter, the samples were triturated using a fire-polished Pasteur pipette and the cell suspensions were passed through a 40- μ m Nylon cell strainer (Nest, Wuxi, China). Afterward, the cell suspensions were cultured in Dulbecco's modified Eagle's medium (DMEM; Hyclone, Logan, UT, USA) supplemented with 20% fetal calf serum after being centrifugated at 1000 rpm. The culture medium was replaced every 2–3 days.

After 10–12 days, immature oligodendrocytes were collected by shaking overnight at 230 rpm. Then, the cell suspensions were pre-seeded for 30 min at 37 °C under 5% CO₂ condition to remove contaminating astrocytes and microglia. Afterward, floating cells were plated on poly-L-ornithine-coated (Sigma-Aldrich, Munich, Germany) cover slips or culture plates (1×10^5 cells/ml) and cultured in DMEM supplemented with 2% B27 (Gibco, Grand Island, NY, USA), 10 ng/ml basic fibroblast growth factor (bFGF, Peprotech, Rocky Hill, NJ, USA), and 10 ng/ml platelet-derived growth factor (PDGF, Peprotech, Rocky Hill, NJ, USA). Thereafter, the purity of cells was determined by co-labelling of NG2 and PDGF α R using immunostaining.

Hepcidin was firstly dissolved in 0.01 M PBS (pH 7.4) and then diluted with culture medium with the final concentration of 0.5 μ M for in vitro experiments. The control or vehicle group was added the same volume of 0.01 M PBS (pH 7.4) as the hepcidin group.

HE Staining

Hematoxylin and eosin (HE) staining was performed to assess the injury and necrosis status of spinal cord after SCI [28]. Briefly, spinal cord sections were sliced using a freezing microtome, washed with distilled water, incubated in

hematoxylin staining solution for 10 min, then rinsed with distilled water 3 times, differentiated in 0.1% hydrochloric acid-ethanol for 25 s, blued in 0.01 M PBS for 45 min followed by 95% alcohol washing for 5 s, thereafter immersed in eosin staining solution for 1 min, dehydrated with 95% alcohol, cleared with xylene, and finally mounted on glass slides. Images were captured using a light microscope (Carl Zeiss, Weimar, Germany), and analyzed by individual investigators blinded to group assignment using an Image J software (ImageJ 1.8, NIH, USA).

Perl's Blue Staining

Perl's blue staining was applied to exhibit iron deposition as previously described [1]. The T10 spinal cord segments containing the injured epicenter and surrounding uninjured tissues (6 mm = 3 mm either side from the injury epicenter) were collected for preparing paraffin sections according to the standard procedures. Paraffin sections (5 μ m) were deal with a graded ethanol series, immersed in xylene, and rehydrated in PBS. Afterward, specimens were incubated in Perls' staining solution (comprising equal parts of potassium ferrocyanide and HCL) for 20 min. Subsequently, the samples were rinsed with Milli-Q water and stained cell nuclei with Fast Red solution for 5–10 min, dehydrated, cleared in xylem, and mounted on glass slides. Images were photographed by a light microscope (Carl Zeiss, Weimar, Germany) and analyzed by individual investigators blinded to group assignment using an ImageJ software (ImageJ 1.8, NIH, USA).

ROS Measurement

Reactive oxygen species (ROS) levels were measured by a ROS assay kit in accordance with the manufacturer's instruction (cat. no. S0033S, Beyotime, Shanghai, China). Primary OPCs were collected and homogenized on ice. Then, each sample was loaded with 500 μ l 10 μ M DCFH-DA and incubated in the dark at 37 °C for 20 min. Afterward, the loading buffer was replaced and washed to eliminate residual DCFH-DA. Subsequently, the samples were immediately measured using a flow cytometer (ACEA Biosciences Inc., San Diego, CA, USA) with an argon laser (488 nm).

IHC

For immunostaining, sections were incubated in 4% paraformaldehyde for 30 min at room temperature and permeabilized with 0.3% Triton-X 100 (Sigma-Aldrich, St. Louis, MO) in PBS. Then, samples were incubated in the following primary antibodies overnight at 4 °C after being blocked with 5% bovine serum albumin (BSA, Sigma-Aldrich, St. Louis, MO), anti-CC1 (cat. no. OP44, Sigma-Aldrich, Munich,

Germany), anti-DMT1 (cat. no. PA5-35136, Thermo Fisher Scientific, Waltham, MA, USA), anti-TfR (cat. no. PA5-116065, Thermo Fisher Scientific, Waltham, MA, USA), anti-NG2 (cat. no. MAB5384-I, Sigma-Aldrich, Munich, Germany), and anti-PDGFR α (cat. no. ab32570, Abcam, Cambridge, UK). On the second day, the samples were immersed in Alexa Fluor® 555 or 488-conjugated secondary antibody (1:100; cat. nos. A0453 and A0423; Beyotime Institute of Biotechnology, Beijing, China) for 2 hours at room temperature. The cell nuclei were counterstained with 4'-6-diamidino-2-phenylindole (DAPI; Beyotime, Shanghai, China) for 10 min at room temperature. Thereafter, the specimens were mounted onto glass slides, and images were captured using a confocal microscope (Carl Zeiss, LSM780, Weimar, Germany) and examined by individual investigators blinded to group assignment using a Zen 2011 software (Carl Zeiss, Weimar, Germany).

For immunohistochemistry, slices were dewaxed and antigen-repaired according to the standard procedures [29]. Then, samples were immersed in endogenous peroxidase for 10 min. Afterward, the specimens were immersed in anti-CC-1 (cat. no. SAB4501438, Sigma-Aldrich, Munich, Germany) primary antibody overnight at 4 °C after being blocked with 5% BSA dissolved in 0.3% Triton-X 100 (Sigma-Aldrich, St. Louis, MO). After being washed, they were incubated in horseradish peroxidase (HRP)-conjugated goat anti-rabbit immunoglobulin G (ZSGB-BIO, Beijing, China). Then, the 3-diaminobenzidine (DAB) kit was employed to show the positive cells in brown color. Afterward, the sections were stained with hematoxylin and dehydrated with ethanol and xylene to mount onto glass slides. Images were photographed by a light microscope (Carl Zeiss, Weimar, Germany), and analyzed by individual investigators blinded to group assignment using an Image J software (ImageJ 1.8, NIH, USA). For each sample, six sections were stained, analyzed, calculated and reported as the average of four independent measurements.

TEM

Transmission electron microscopy (TEM) was performed to visualize the ultrastructure of myelin sheath and mitochondria status in each group, as previously described [1]. In brief, the samples containing the injured epicenter and surrounding uninjured tissues (2 mm = 1 mm either side from the epicenter) were firstly fixed in 1.25% glutaraldehyde overnight after perfusion. Then, the samples were post-fixed in 1.25% glutaraldehyde 3 days at 4 °C. Thereafter, the specimens were washed and incubated in 1% citric acid (OsO4) for 2 h. Afterward, uranyl acetate was used for redyeing, and gradient acetone was used for dehydration. Then, an ultramicrotome (EM UC7, Leica, IL, USA) was used for slicing before the samples were infiltrated with propylene

oxide and embedded by epoxy. Images were photographed using a transmission electron microscope (Hitachi HT7700, Tokyo, Japan). At least three independent samples per group were analyzed by individual investigators blinded to group assignment using an Image J software (ImageJ 1.8, NIH, USA) to exhibit the myelin sheath thickness.

Western Blot

The T10 spinal cord segments containing the injured epicenter and surrounding uninjured tissues (0.5 cm = 0.25 cm either side from the epicenter) were immediately collected after decapitation on day 7 post-SCI. The tissues were collected after being homogenized and the protein concentrations of each sample were measured by a bicinchoninic acid (BCA) method (Beyotime, Shanghai, China). A total of 50 µg proteins were separated by 8 or 10% SDS-PAGE under reducing conditions and electro-blotted to polyvinylidene difluoride (PVDF, Roche, Indianapolis, IN, USA) membranes. Then, the membranes were blocked with 5% non-fat dry milk (Beyotime, Shanghai, China) in tris-buffered saline (TBS) with Tween-20 (TBST) for 2 h at room temperature. Afterward, the samples were submerged in primary antibodies, anti-dMBP (cat. no. MBS618031, MybioSource, San Diego, CA, USA), anti-DMT1 (cat. no. PA5-35136, Thermo Fisher Scientific, Waltham, MA, USA), anti-APP antibody (cat. no. MAB348, Sigma-Aldrich, Munich, Germany), anti-TfR (cat. no. MA5-32500, Thermo Fisher Scientific, Waltham, MA, USA), or anti-GAPDH (cat. no. AF0006; Beyotime, Shanghai, China) overnight at 4 °C. On the next day, the membrane was submerged in corresponding horseradish peroxidase (HRP)-conjugated secondary antibodies after being washed with TBST. All membranes were visualized by a ChemiDoc™ XRS+ imaging system (Bio-Rad, California, USA) using the WesternBright ECL Kits (Beyotime, Shanghai, China). Densitometric density of each membrane was determined using an Image Lab™ software (Bio-Rad, California, USA), and analyzed by individual investigators blinded to group assignment.

RT-qPCR

Total RNA was extracted using a TaKaRa MiniBEST Universal RNA Extraction Kit (cat no. 9767, TaKaRa, Tokyo, Japan) in accordance with the manufacturer's instructions after primary OPCs were gathered from each group. Then,

a total of 1 µg RNA was reversely transcribed into cDNA using a PrimeScript RT reagent Kit with gDNA Eraser (cat. no. RR0047A, TaKaRa, Tokyo, Japan). Subsequently, qPCR was performed using the CFX96 System (Bio-Rad, CA, USA) with SYBR Premix Ex TaqII (Tli RNaseH Plus; cat. no. RR820A, TaKaRa, Tokyo, Japan) under the following condition: 95 °C for 30 s, 40 cycles at 95 °C for 5 s and 60 °C for 30 s. Relative mRNA levels were normalized to GAPDH and analyzed using the $2^{-\Delta\Delta C_q}$ method. Primer sequences used in the present study are listed in Table 1.

LDH Detection

Lactate dehydrogenase (LDH) releasing levels were evaluated using a LDH assay kit (Nanjing Jiancheng Bioengineering Inc., Nanjing, China) according to the manufacturer's instructions to assess cytotoxicity. Briefly, the supernatants were firstly collected, then neurospheres were lysed with 2% Triton X-100 for 15 min on ice to release all LDH from the cytoplasm. LDH released from cell lysates was measured to be the maximal LDH release and was used as positive controls. LDH releasing levels were determined by a microplate reader (Thermo Fisher Scientific, Waltham, MA, USA) at the wavelength of 450 nm, and data were presented as the content of LDH (U/L) released in the medium.

Cell Viability Assay

The cell viability was determined by a cell counting kit-8 (CCK8; Dojindo, Tokyo, Japan), which uses a water-soluble tetrazolium salt to quantify the number of live cells by producing an orange formazan dye upon bio-reduction in the presence of an electron carrier. Briefly, 100 µl of cell suspension (1×10^5 cells/well) was dispensed in a 96-well cell culture cluster, then incubated in 10% (v/v) CCK8 solution for at 37 °C for 2.5 h. Then, the absorbance of the culture medium at a test wavelength of 450 nm was determined using a microplate reader (Thermo Fisher Scientific, Waltham, MA, USA) and a reference wavelength of 630 nm as well.

Statistical Analysis

All data were expressed as mean ± SEM. The statistical analyses were implemented using SPSS 18.0 software (SPSS, Inc., Chicago, IL, USA). For statistical data collected

Table 1 Primer sequences for RT-qPCR

Target genes	Forward primer sequence (5'-3')	Reverse primer sequence (5'-3')
DMT1	TGATCCTGACCCGGTCTATC	CAATCCTCCAGCCTATTCCA-
TfR	CTAGTATCTTGAGGTGGGAGGAAGAG	GAGAATCCCAGTGAGGGTCAGA
GAPDH	GACAACCTTGGCATTGTGG	ATGCAGGGATGATGTTCTG

Fig. 1 Hepcidin facilitated functional recovery through reducing iron deposition and facilitating the survival of oligodendrocytes after SCI. **A** Histogram demonstrating the Basso, Beattie, and Bresnahan (BBB) score in each group on days 7, 35, and 56 following SCI. $N = 7$, two-way ANOVA followed by Tukey's post hoc test. **B** HE staining showing the status of spinal cord on day 7 following SCI. Scale bars: 200 μm . $N = 4$ per group. **C** Perl's blue staining images depicting the iron accumulation in the epicenter of injured spinal cord on day 7 in different groups. Scale bar: 50 μm . $N = 4$ per group. **D** Immunohistochemistry images indicating the CC1⁺ cells in the epicenter of injured spinal cord in each group on day 7. Scale bar: 50 μm . **E** Bar chart illustrating the number of CC1⁺ cells from **D**. $N = 4$, one-way ANOVA followed by Tukey's post hoc test

from each independent group at different time points were analyzed using two-way analysis of variance (ANOVA), followed by Turkey's post hoc test. For data with a single time point, multiple comparisons were performed by one-way ANOVA, followed by Turkey's post hoc test in case of the data with a normal distribution using a Shapiro–Wilk normality test. A $p < 0.05$ was considered to be statistical difference.

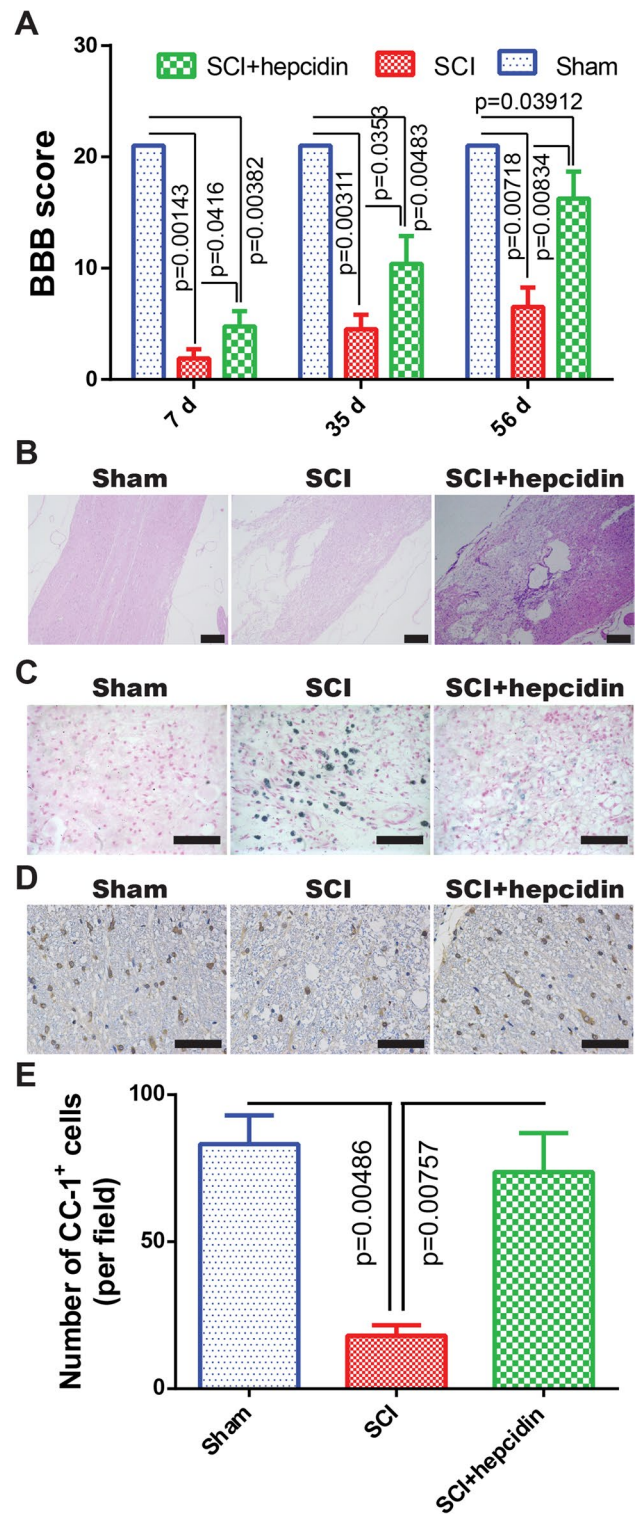
Results

Hepcidin Improved Functional Recovery Through Decreasing Iron Accumulation and Promoting Oligodendrocyte Survival After SCI in Rats

To assess the role of hepcidin in functional recovery after SCI, the BBB score was firstly performed. The results demonstrated that the BBB score of rats in SCI+hepcidin group was significantly higher than that in SCI group from day 7 to 56 (Fig. 1A). Then, the HE staining images showed that the administration of hepcidin obviously decreased the spinal cord atrophy that was apparently observed in the epicenter of injured spinal cords on day 7 post-SCI (Fig. 1B). And, the application of hepcidin evidently decreased the iron content using Perl's blue staining, whose level was clearly increased in the epicenter of injured spinal cord following SCI (Fig. 1C). Furthermore, the immunohistochemistry images depicted the number of CC1⁺ cells were greatly decreased after SCI, while the administration of hepcidin obviously abrogated this effect (Fig. 5D, E). Collectively, these results illustrated that hepcidin facilitated functional recovery by reducing iron deposition and facilitating oligodendrocytes survival after SCI.

Hepcidin Decreased WMI Through Mitigating Ferroptosis on Day 7 After SCI in Rats

Previous results had indicated that hepcidin promoted oligodendrocytes following SCI, the myelin sheath thickness was determined using TEM. The images demonstrated that



the myelin sheath thickness was significantly decreased after SCI, while the application of hepcidin obviously increased the myelin sheath thickness (Fig. 2A, B). Meanwhile, the immunoblot bands presented that the expression of degraded myelin basic protein (dMBP) and amyloid precursor protein (APP) was predominantly

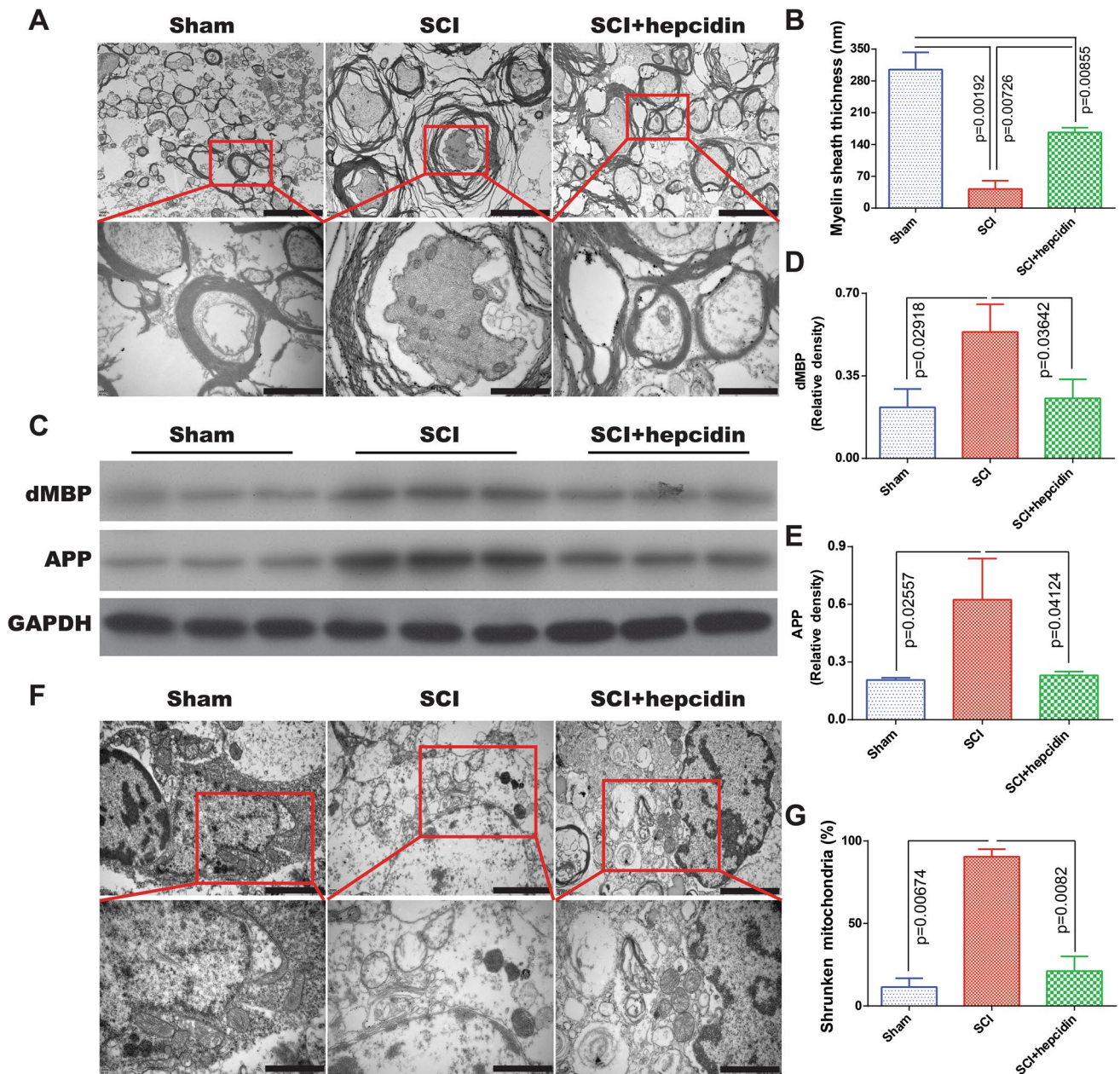


Fig. 2 Hepcidin reduced white matter injury (WMI) by alleviating ferroptosis post-SCI. **A** TEM images showcasing the myelin sheath thickness in each group on day 7 post-SCI. Scale bars: 5 μ m; 1 μ m for enlarged inserts. **B** Bar graph showing the myelin sheath thickness from **A**. $N = 4$, one-way ANOVA followed by Tukey's post hoc test. **C** Immunoblot bands representing the expression levels of dMBP and APP in various groups. GAPDH was loaded as an internal control. **D**,

E Semi-quantification of the expression of dMBP (**D**) and APP (**E**) from **C**. $N = 3$, one-way ANOVA followed by Tukey's post hoc test. **F** TEM images showing the morphological changes of mitochondria in each group on day 7 post-SCI. Scale bars: 5 μ m; 1 μ m for enlarged inserts. **G** Histogram summarizing the percentage of shrunken mitochondria from **F**. $N=4$, one-way ANOVA followed by Tukey's post hoc test.

increased after SCI, whereas this effect was substantially abolished with the treatment of hepcidin (Fig. 2C–E). Considering that iron accumulation always results in ROS production to induce ferroptosis [21], the status of ferroptosis was evaluated by TEM assays in each group. The TEM images illustrated that the proportion of shrunken

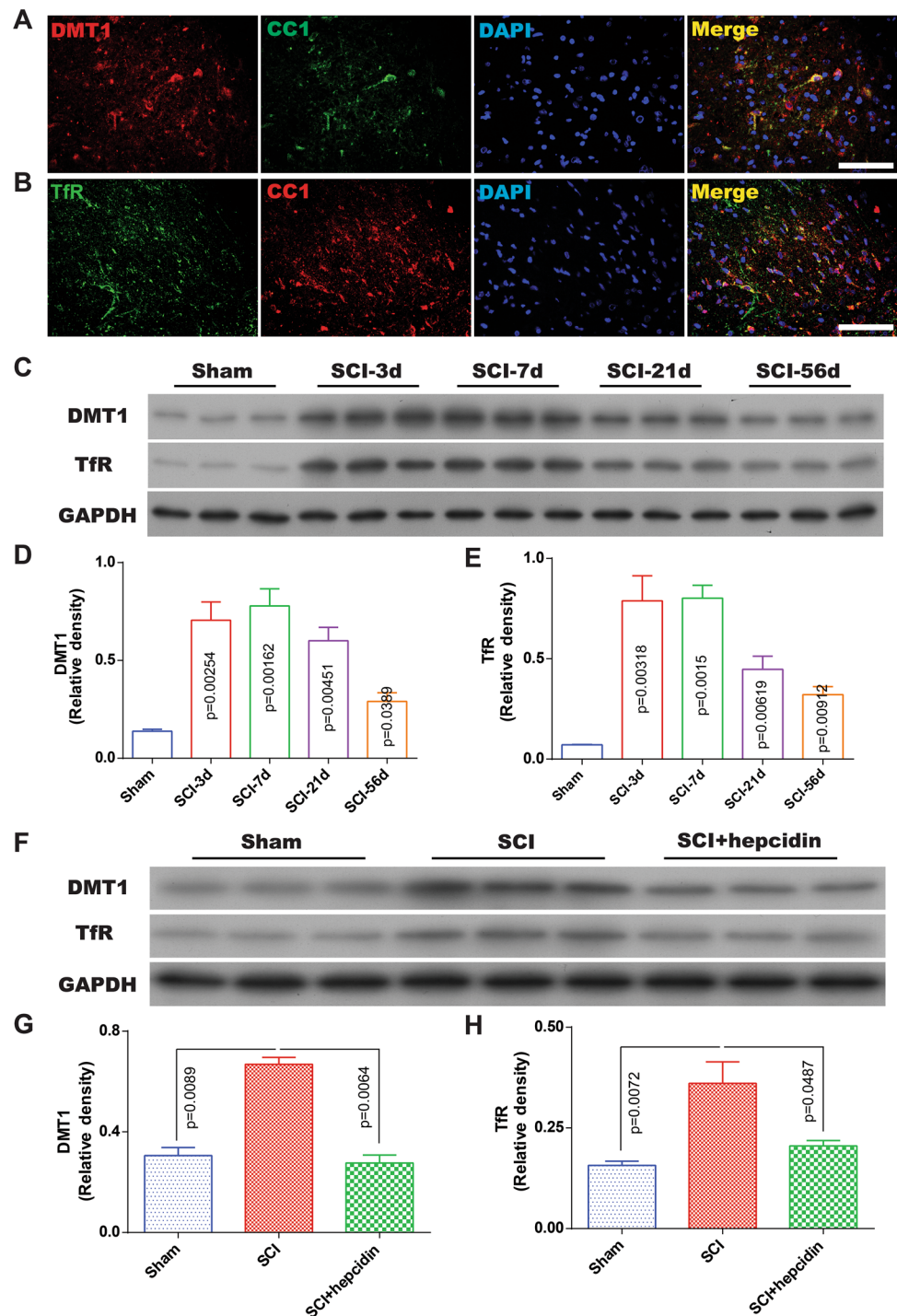
mitochondria was surely elevated after SCI, while the application of hepcidin profoundly declined the percentage of depauperated mitochondria (Fig. 2F, G). Taken together, these results demonstrated that SCI triggered WMI via ferroptosis, and this phenomenon was partially compromised with the treatment of hepcidin.

Hepcidin Compromised Ferroptosis by Downregulating the Expression of DMT1 and TfR Post-SCI

Previous studies have demonstrated that cultured astrocytes and neurons expressed TfR and DMT1 [24, 25], while the expression of TfR and DMT1 was not elucidated. Here, the expression of TfR and DMT1 was determined using

immunostaining. The representative images illustrated that DMT1 and TfR expressed in CC1⁺ cells (Fig. 3A, B). Thereafter, the immunoblot bands demonstrated that the expression of DMT1 and TfR was gradually increased, and reached the peak on day 7 post-SCI (Fig. 3C–E). And, the expression of DMT1 and TfR was still stayed at high level at least on day 56 (Fig. 3C–E). In addition, the administration of hepcidin significantly reduced the expression of DMT1 and

Fig. 3 Hepcidin mitigated ferroptosis via decreasing the expression of DMT1 and TfR after SCI. **A** Immunostaining images depicting the co-labeling of DMT1 (red) and CC1 (green) in each group on day 7 post-SCI. Scale bar: 50 μ m. **B** Immunostaining images depicting the co-localization of TfR (green) and CC1 (red) in each group on day 7 after SCI. Scale bar: 50 μ m. **C** Immunoblot bands depicting the expression levels of DMT1 and TfR on days 3, 7, 21, and 56 post-SCI. GAPDH was loaded as an internal control. **D, E** Semi-quantification of the expression of DMT1 (**D**) and TfR (**E**) from **C**. $N = 3$, one-way ANOVA followed by Tukey's post hoc test. **F** Immunoblot bands showing the expression levels of DMT1 and TfR in different groups post-SCI. GAPDH was loaded as an internal control. **G, H** Semi-quantification of the expression of DMT1 (**G**) and TfR (**H**) from **F**. $N = 3$, one-way ANOVA followed by Tukey's post hoc test



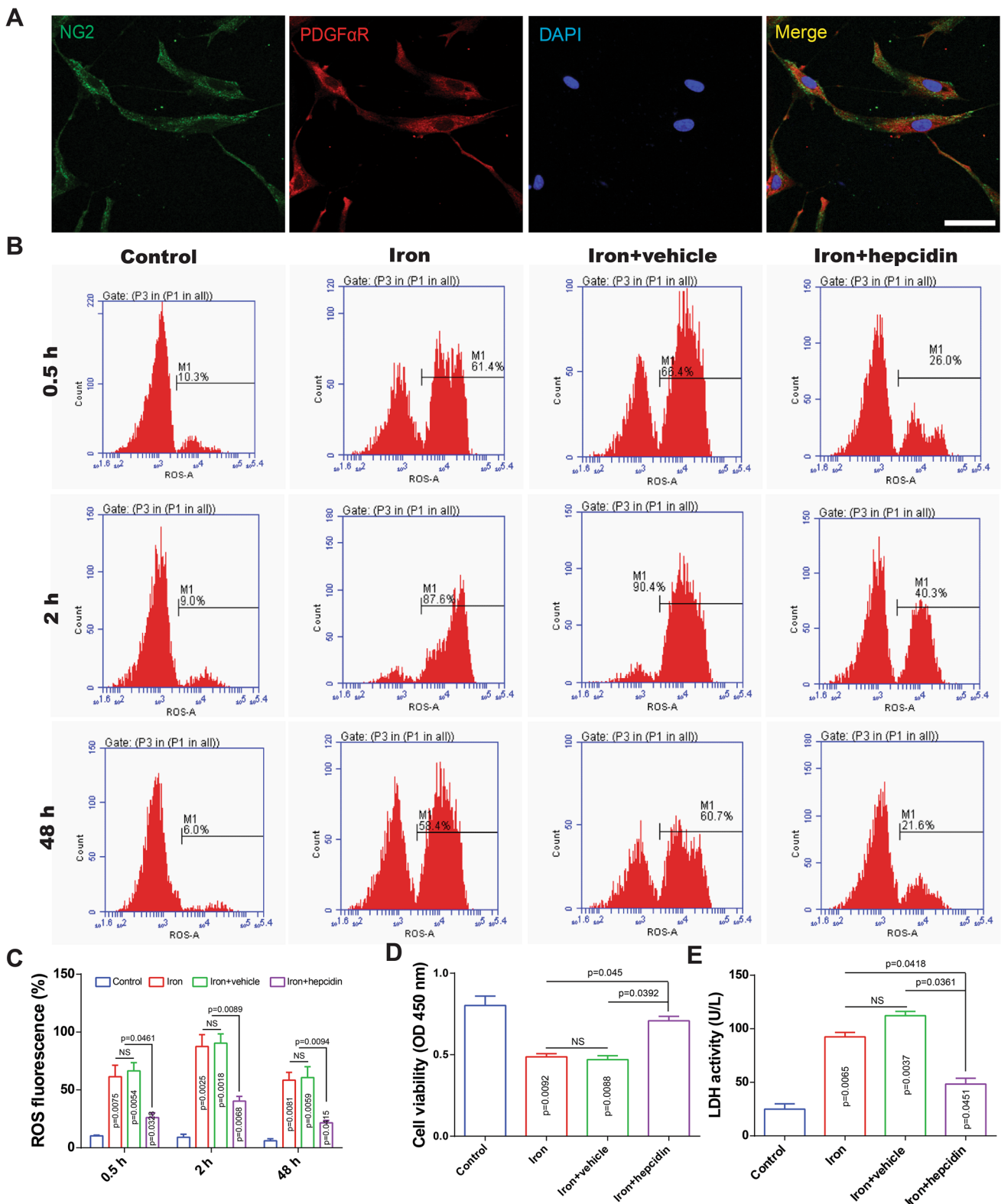
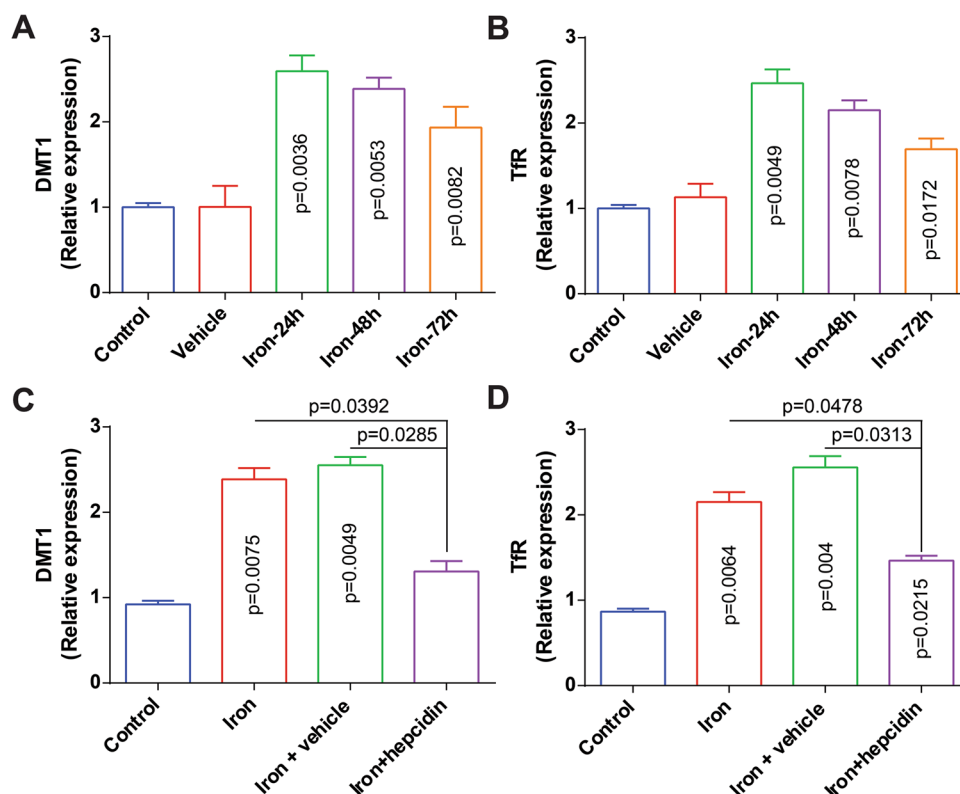


Fig. 4 Hepcidin reduced ROS accumulation to increase cell viability and reduce LDH releasing in vitro. **A** Immunostaining images demonstrating the expression of NG2 (green) and PDGFαR (red) in primary OPCs. Scale bars: 20 μm. **B** Representational images demonstrating the ROS accumulation using flow cytometry. **C** Histogram summarizing

the percentage of ROS fluorescence from **A**. $N = 3$, two-way ANOVA followed by Tukey’s post hoc test. **D** Bar graph illustrating the absorbance value at 450 nm in each group. $N = 6$, one-way ANOVA followed by Tukey’s post hoc test. **E** LDH releasing assays in each group. $N = 6$, one-way ANOVA followed by Tukey’s post hoc test

Fig. 5 Hepcidin decreased the gene expression of DMT1 and TfR to mitigate OPCs ferroptosis resulting from iron overload. **A, B** Quantification of the gene expression of DMT1 (**A**) and TfR (**B**) determined by RT-qPCR in each group at different time points. $N = 4$. **C, D** Quantification of the gene expression of DMT1 (**C**) and TfR (**D**) assessed using RT-qPCR in each group. $N = 4$, one-way ANOVA followed by Tukey's post hoc test



TfR, which was remarkably increased after SCI, on day 7 (Fig. 3F–H). Taken together, these results showcased that TfR and DMT1 expressed in oligodendrocytes and hepcidin reduced ferroptosis through decreasing the expression of DMT1 and TfR after SCI on day 7.

Hepcidin Decreased ROS Deposition to Increase Cell Viability and Reduce LDH Releasing in OPCs In Vitro

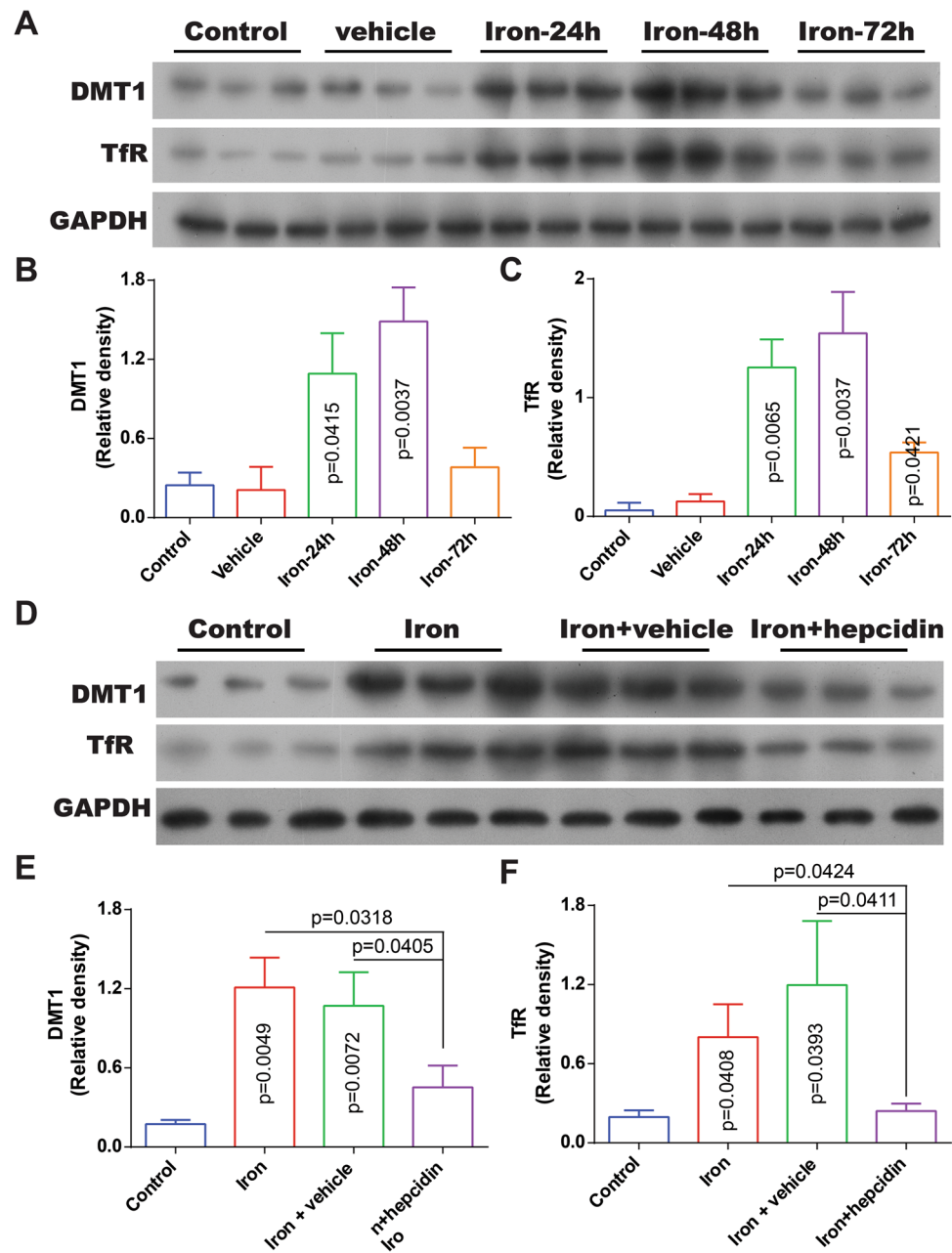
The above findings illustrated that the application of hepcidin reduced ferroptosis. Whether ferroptosis occurred in the oligodendrocytes, the primary OPCs was firstly cultured. The immunostaining images illustrated that the cultured cells expressed NG2 and PDGF α R (Fig. 4A), indicating that the cultured cells were oligodendrocytes. Our previous study has represented that the iron concentration was about 30 μ M/g in the epicenter of injured spinal cords [1], then 20 μ M FeCl₃ was used to simulate the iron content in vitro experiments. The results revealed that the ROS level was prominently increased from 0.5 to 48 h (Fig. 4B, C), while the application of hepcidin markedly decreased the content of ROS (Fig. 4B, C). At the same time, the cell viability was clearly decreased in group with the addition of 20 μ M FeCl₃, while it was greatly reversed with the treatment of hepcidin in OPCs reflecting by absorbance value at 450 nm (Fig. 4D). Subsequently, the LDH releasing assays illustrated that the content of LDH was profoundly increased with the

addition of 20 μ M FeCl₃, whereas the administration of hepcidin partially overturned this effect (Fig. 4E). Collectively, these results demonstrated that iron evoked ferroptosis to decreased cell viability and increasing LDH activity, while the application of hepcidin markedly abolished this effect to minimize OPCs ferroptosis.

Hepcidin Alleviated Ferroptosis Through Reducing the Expression of DMT1 and TfR in OPCs In Vitro

The in vitro results supported that hepcidin reduced OPCs ferroptosis, and the mechanism was investigated based on the in vivo results that hepcidin mitigated ferroptosis through downregulating the expression of DMT1 and TfR. Firstly, the results indicated that the gene expression of DMT1 and TfR was significantly upregulated with the addition of 20 μ M FeCl₃ from 24 to 72 h (Fig. 5A, B). Meanwhile, the administration of hepcidin clearly reduced the gene expression of DMT1 and TfR (Fig. 5C, D). Next, the immunoblot bands presented that the protein expression of DMT1 and TfR was obviously elevated with the treatment of 20 μ M FeCl₃ from 24 to 72 h (Fig. 6A–C). And, the application of hepcidin evidently downregulated the protein expression of DMT1 and TfR (Fig. 6D–F). Taken together, these results demonstrated that hepcidin inhibited OPCs ferroptosis by downregulating the expression of DMT1 and TfR.

Fig. 6 Hepcidin reduced the expression of DMT1 and TfR to mitigate OPC ferroptosis deriving from iron accumulation. **A** Immunoblot bands representing the expression levels of DMT1 and TfR in each group at different time points. GAPDH was loaded as an internal control. **B, C** Semi-quantification of the expression of DMT1 (**B**) and TfR (**C**) from **A**. $N = 4$, one-way ANOVA followed by Tukey's post hoc test. **D** Immunoblot bands representing the expression levels of DMT1 and TfR in each group. GAPDH was loaded as an internal control. **E, F** Semi-quantification of the expression of DMT1 (**E**) and TfR (**F**) from **D**. $N = 4$, one-way ANOVA followed by Tukey's post hoc test



Discussion

SCI usually results in permanent or long-lasting neurological impairments, at least in part, ascribing to WMI [1, 2]. Oligodendrocytes are rich in unsaturated fatty acid [4] and susceptible to ferroptosis-induced damage [16]. Hepcidin holds the capacity of reducing iron content, thereafter mitigating ROS production and ferroptosis. However, the effect of hepcidin on ferroptosis in the epicenter of spinal cord remains elusive. Here, the results offer evidence that the administration of hepcidin reduces iron accumulation to promote oligodendrocytes survival and to decrease spinal cord atrophy, therefore facilitating functional recovery.

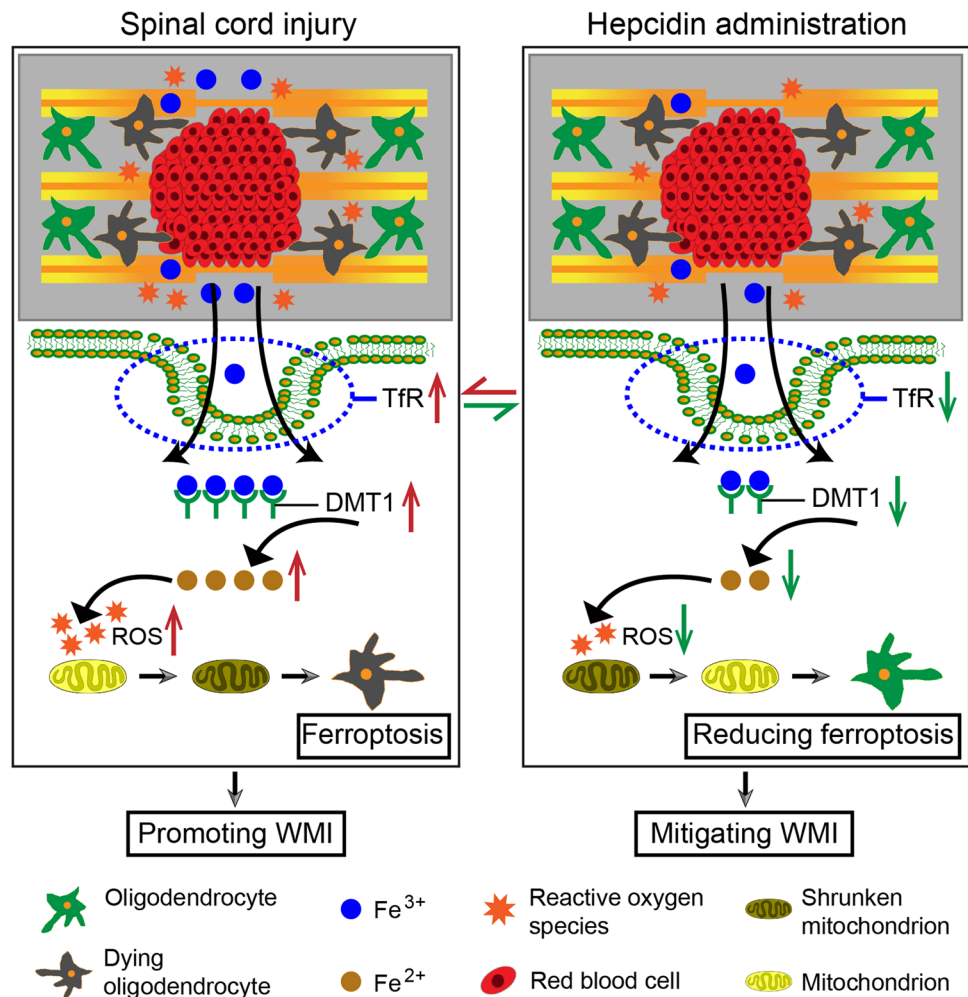
With the increased number of oligodendrocytes in the epicenter of spinal cord, the WMI is evidently decreased due to attenuating ferroptosis. Subsequently, the results uncover that the expression of DMT1 and TfR is expressed in CC1⁺ cells. The expression of DMT1 and TfR is significantly increased, while the phenomenon is obviously neutralized with the administration of hepcidin in the epicenter of spinal cord after SCI. Afterward, the application of hepcidin downregulates increased ROS level, which is evidently increased with the treatment of 20 μ M FeCl₃, thereafter increasing cell viability and reducing LDH activity through downregulating the expression of DMT1 and TfR to inhibit ferroptosis in OPCs (Fig. 7).

The present study provides evidence that the application of hepcidin facilitates oligodendrocytes survival to alleviate WMI via minimizing the expression of DMT1 and TfR.

Iron is an essential cofactor for the generation of cholesterol and phospholipids that are essential ingredients for efficient maturation of OPCs [30]. With the process of myelination, the expression of DMT1 and TfR, two of iron uptake proteins, is elevated to promote iron deposition resulting in OPC maturation [21, 31], which might be the reason why the expression of DMT1 and TfR remains higher level on day 56 post-SCI. Meanwhile, our previous study has indicated that SCI usually evokes iron accumulation in the epicenter of injured spinal cord [1], which positively induces the iron deposition in cytoplasm through the upregulation of DMT1 and TfR [32, 33]. Thereafter, the ROS level is significantly increased due to iron accumulation to trigger ferroptosis [1, 33], which is in consistency with the results that the ROS level is evidently elevated to evoke ferroptosis in oligodendrocytes with the administration of 20 μM FeCl_3 in present study. Thence, exploring approach to downregulate the expression of DMT1 and TfR is a feasible method to reduce oligodendrocytes ferroptosis, therefore alleviating WMI after SCI.

Here, our results demonstrates that hepcidin is a suitable candidate to reduce ferroptosis through decreasing the expression of DMT1 and TfR. Hepcidin is a secreted peptide hormone, and firstly isolated from blood and urine in human [34, 35]. Previous studies have reported hepcidin is dramatically downregulated in hippocampal lysates from mouse Alzheimer's disease (AD) brains along with the presence of iron overload [36, 37], suggesting that the administration of hepcidin is a suitable regimen for the reduction of iron concentration in CNS. And, SCI usually triggers iron accumulation not only in the epicenter of spinal cord [1, 17, 26, 38] but also in the motor cortex [20] both in animal SCI model and human. However, the application of hepcidin obviously decreases the iron content to downregulate ferroptosis in the epicenter of spinal cord following SCI. Meanwhile, another reason for the administration of hepcidin promoting functional recovery is that hepcidin holds the ability of inhibiting inflammatory process due to reducing IL-6 expression and secretion in astrocytes and microglia [39], indicating that hepcidin could serve as a neuroinflammatory suppressor. Together, the application of

Fig. 7 Schematic illustration for the potential therapeutic effect of hepcidin on ferroptosis following SCI and the underlying mechanism



hepcidin exerts neuroprotective effect, at least in part, due to repressing ferroptosis and neuroinflammation.

Some limitations exist in the present study. Firstly, the most recent study has indicated that mRNA-miRNA-lncRNA network is involved in ferroptosis after SCI [40]. And, some miRNAs or related lncRNA promote functional recovery, such as miR-672-3p and the cascade of lncGm36569/miR-5627-5P, through suppressing ferroptosis suppressor protein 1 (FSP1) after SCI in rats [41, 42]. Furthermore, this study is a routine study without unique and innovative methods. Hence, some future research needs to be performed to elucidate role of the mRNA-miRNA-lncRNA network in regulating ferroptosis using more innovative approaches following SCI.

Conclusions

In conclusion, the present study provides direct evidence that the administration of hepcidin significantly downregulates iron overload and ferroptosis in the epicenter of spinal cord, therefore facilitating oligodendrocytes survival to alleviating WMI following SCI in rats. With the reduction of WMI, the functional recovery is obviously improved post-SCI. This study enlarges the therapeutic scope of hepcidin on SCI, and even for other CNS diseases with the presence of ferroptosis.

Authors' Contribution Jiantao Shi, Xingsen Xue, and Linbo Yuan performed most of the experiments, with assistance from Guanjian He, Zhouyang Jiang, Long Wang, Jiali Zhang, and Hong Su. Zhouyang Jiang and Long Wang analyzed the results and edited figures. Jiantao Shi, Xingsen Xue, and Linbo Yuan performed SCI model and statistical analysis. Guanjian He and Jiali Zhang performed cell culture and treatments. Jiantao Shi, Xingsen Xue, and Jishu Xian performed immunoblotting and immunostaining. Jiantao Shi wrote preliminary draft of the manuscript. Chuhua Fu designed experiments and revised the manuscript. Shengli Hu made the hypothesis and revised the manuscript. All authors approved final version of the manuscript.

Funding This work was supported by grants from the National Natural Science Foundation of China (approval no. 81471261) and Natural Science Foundation of Chongqing (approval no. cstc2018jcyjAX0080).

Data Availability The data that support the findings of this study are available from the corresponding author upon reasonable request.

Declarations

Research Involving Animals The animal experiment procedures were implemented according to the China's animal welfare legislation for the protection of animals used for scientific purposes. And, this work was supervised by the Ethics Committee of the Southwest Hospital, Third Military Medical University (Army Medical University) for the use of laboratory animals (approval no. AMUWEC20210017).

Informed Consent Not applicable.

Consent to Participate Not applicable.

Consent for Publication Not applicable.

Conflict of Interest The authors declare no competing interests.

References

- Ge H, Xue X, Xian J, Yuan L, Wang L, Zou Y, Zhong J, Jiang Z, et al (2022) Ferrostatin-1 alleviates white matter injury via decreasing ferroptosis following spinal cord injury. *Mol Neurobiol* 59(1):161–176. <https://doi.org/10.1007/s12035-021-02571-y>
- Krupa P, Svobodova B, Dubisova J, Kubinova S, Jendelova P, Machova Urdzikova L (2019) Nano-formulated curcumin (Lipodisq™) modulates the local inflammatory response, reduces glial scar and preserves the white matter after spinal cord injury in rats. *Neuropharmacology* 155:54–64. <https://doi.org/10.1016/j.neuropharm.2019.05.018>
- Yuan J, Liu W, Zhu H, Chen Y, Zhang X, Li L, Chu W, Wen Z, et al (2017) Curcumin inhibits glial scar formation by suppressing astrocyte-induced inflammation and fibrosis in vitro and in vivo. *Brain Res* 1655:90–103. <https://doi.org/10.1016/j.brainres.2016.11.002>
- Xia Y, Zhao T, Li J, Li L, Hu R, Hu S, Feng H, Lin J (2008) Antisense vimentin cDNA combined with chondroitinase ABC reduces glial scar and cystic cavity formation following spinal cord injury in rats. *Biochem Biophys Res Commun* 377(2):562–566. <https://doi.org/10.1016/j.bbrc.2008.10.024>
- Xia Y, Yan Y, Xia H, Zhao T, Chu W, Hu S, Feng H, Lin J (2015) Antisense vimentin cDNA combined with chondroitinase ABC promotes axon regeneration and functional recovery following spinal cord injury in rats. *Neurosci Lett* 590:74–79. <https://doi.org/10.1016/j.neulet.2015.01.073>
- Hu R, Duan B, Wang D, Yu Y, Li W, Luo H, Lu P, Lin J, et al (2011) Role of acid-sensing ion channel 1a in the secondary damage of traumatic spinal cord injury. *Ann Surg* 254(2):353–362. <https://doi.org/10.1097/SLA.0b013e31822645b4>
- Hu R, Sun H, Zhang Q, Chen J, Wu N, Meng H, Cui G, Hu S, et al (2012) G-protein coupled estrogen receptor 1 mediated estrogenic neuroprotection against spinal cord injury. *Crit Care Med* 40(12):3230–3237. <https://doi.org/10.1097/CCM.0b013e3182657560>
- Chen J, Hu R, Ge H, Duanmu W, Li Y, Xue X, Hu S, Feng H (2015) G-protein-coupled receptor 30-mediated antiapoptotic effect of estrogen on spinal motor neurons following injury and its underlying mechanisms. *Mol Med Rep* 12(2):1733–1740. <https://doi.org/10.3892/mmr.2015.3601>
- Li L, Xiong ZY, Qian ZM, Zhao TZ, Feng H, Hu S, Hu R, Ke Y, et al (2014) Complement C5a is detrimental to histological and functional locomotor recovery after spinal cord injury in mice. *Neurobiol Dis* 66:74–82. <https://doi.org/10.1016/j.nbd.2014.02.008>
- Chu W, Yuan J, Huang L, Xiang X, Zhu H, Chen F, Chen Y, Lin J, et al (2015) Valproic acid arrests proliferation but promotes neuronal differentiation of adult spinal NSPCs from SCI rats. *Neurochem Res* 40(7):1472–1486. <https://doi.org/10.1007/s11064-015-1618-x>
- Chen F, Wang H, Xiang X, Yuan J, Chu W, Xue X, Zhu H, Ge H, et al (2014) Curcumin increased the differentiation rate of neurons in neural stem cells via wnt signaling in vitro study. *J Surg Res* 192(2):298–304. <https://doi.org/10.1016/j.jss.2014.06.026>
- Hu SL, Luo HS, Li JT, Xia YZ, Li L, Zhang LJ, Meng H, Cui GY, et al (2010) Functional recovery in acute traumatic spinal cord injury after transplantation of human umbilical cord mesenchymal stem cells. *Crit Care Med* 38(11):2181–2189. <https://doi.org/10.1097/CCM.0b013e3181f17c0e>
- Liu S, Zhang W, Yang L, Zhou F, Liu P, Wang Y (2021) Overexpression of bone morphogenetic protein 7 reduces

- oligodendrocytes loss and promotes functional recovery after spinal cord injury. *J Cell Mol Med* 25(18):8764–8774. <https://doi.org/10.1111/jcmm.16832>
14. Duncan GJ, Manesh SB, Hilton BJ, Assinck P, Plemel JR, Tetzlaff W (2020) The fate and function of oligodendrocyte progenitor cells after traumatic spinal cord injury. *Glia* 68(2):227–245. <https://doi.org/10.1002/glia.23706>
 15. Pukos N, Goodus MT, Sahinkaya FR, McTigue DM (2019) Myelin status and oligodendrocyte lineage cells over time after spinal cord injury: what do we know and what still needs to be unwrapped? *Glia* 67(11):2178–2202. <https://doi.org/10.1002/glia.23702>
 16. Jhelum P, Santos-Nogueira E, Teo W, Haumont A, Lenoël I, Stys PK, David S (2020) Ferroptosis mediates cuprizone-induced loss of oligodendrocytes and demyelination. *J Neurosci* 40(48):9327–9341. <https://doi.org/10.1523/jneurosci.1749-20.2020>
 17. Chen Y, Liu S, Li J, Li Z, Quan J, Liu X, Tang Y, Liu B (2020) The latest view on the mechanism of ferroptosis and its research progress in spinal cord injury. *Oxidative Med Cell Longev* 2020:6375938. <https://doi.org/10.1155/2020/6375938>
 18. Li Q, Weiland A, Chen X, Lan X, Han X, Durham F, Liu X, Wan J, et al (2018) Ultrastructural characteristics of neuronal death and white matter injury in mouse brain tissues after intracerebral hemorrhage: coexistence of ferroptosis, autophagy, and necrosis. *Front Neurol* 9:581. <https://doi.org/10.3389/fneur.2018.00581>
 19. Yao X, Zhang Y, Hao J, Duan HQ, Zhao CX, Sun C, Li B, Fan BY, et al (2019) Deferoxamine promotes recovery of traumatic spinal cord injury by inhibiting ferroptosis. *Neural Regen Res* 14(3):532–541. <https://doi.org/10.4103/1673-5374.245480>
 20. Feng Z, Min L, Chen H, Deng W, Tan M, Liu H, Hou J (2021) Iron overload in the motor cortex induces neuronal ferroptosis following spinal cord injury. *Redox Biol* 43:101984. <https://doi.org/10.1016/j.redox.2021.101984>
 21. Qian ZM, Ke Y (2020) Hepcidin and its therapeutic potential in neurodegenerative disorders. *Med Res Rev* 40(2):633–653. <https://doi.org/10.1002/med.21631>
 22. Ganz T (2013) Systemic iron homeostasis. *Physiol Rev* 93(4):1721–1741. <https://doi.org/10.1152/physrev.00008.2013>
 23. Ge XH, Wang Q, Qian ZM, Zhu L, Du F, Yung WH, Yang L, Ke Y (2009) The iron regulatory hormone hepcidin reduces ferroportin 1 content and iron release in H9C2 cardiomyocytes. *J Nutr Biochem* 20(11):860–865. <https://doi.org/10.1016/j.jnutbio.2008.07.014>
 24. Du F, Qian ZM, Luo Q, Yung WH, Ke Y (2015) Hepcidin suppresses brain iron accumulation by downregulating iron transport proteins in iron-overloaded Rats. *Mol Neurobiol* 52(1):101–114. <https://doi.org/10.1007/s12035-014-8847-x>
 25. Du F, Qian C, Qian ZM, Wu XM, Xie H, Yung WH, Ke Y (2011) Hepcidin directly inhibits transferrin receptor 1 expression in astrocytes via a cyclic AMP-protein kinase A pathway. *Glia* 59(6):936–945. <https://doi.org/10.1002/glia.21166>
 26. Shi J, Tang R, Zhou Y, Xian J, Zuo C, Wang L, Wang J, Feng H, et al (2020) Attenuation of white matter damage following deferoxamine treatment in rats after spinal cord injury. *World Neurosurg* 137:e9–e17. <https://doi.org/10.1016/j.wneu.2019.08.246>
 27. Basso DM, Beattie MS, Bresnahan JC (1995) A sensitive and reliable locomotor rating scale for open field testing in rats. *J Neurotrauma* 12(1):1–21. <https://doi.org/10.1089/neu.1995.12.1>
 28. Hu SL, Lu PG, Zhang LJ, Li F, Chen Z, Wu N, Meng H, Lin JK, et al (2012) In vivo magnetic resonance imaging tracking of SPIO-labeled human umbilical cord mesenchymal stem cells. *J Cell Biochem* 113(3):1005–1012. <https://doi.org/10.1002/jcb.23432>
 29. Jiang X, Zhang J, Kou B, Zhang C, Zhong J, Fang X, Huang X, Zhang X, et al (2020) Ambroxol improves neuronal survival and reduces white matter damage through suppressing endoplasmic reticulum stress in microglia after intracerebral hemorrhage. *Biomed Res Int* 2020:8131286. <https://doi.org/10.1155/2020/8131286>
 30. Cheli VT, Correale J, Paez PM, Pasquini JM (2020) Iron metabolism in oligodendrocytes and astrocytes, implications for myelination and remyelination. *ASN neuro* 12:1759091420962681. <https://doi.org/10.1177/1759091420962681>
 31. Cheli VT, Santiago González DA, Marziali LN, Zamora NN, Guitart ME, Spreuer V, Pasquini JM, et al (2018) The divalent metal transporter 1 (DMT1) is required for iron uptake and normal development of oligodendrocyte progenitor cells. *J Neurosci* 38(43):9142–9159. <https://doi.org/10.1523/jneurosci.1447-18.2018>
 32. Zhang L, Wang Z, Song C, Liu H, Li Y, Li J, Yu Y, Wang G, et al (2021) Spinal NR2B phosphorylation at Tyr1472 regulates IRE(-)DMT1-mediated iron accumulation and spine morphogenesis via kalirin-7 in tibial fracture-associated postoperative pain after orthopedic surgery in female mice. *Reg Anesth Pain Med* 46(4):363–373. <https://doi.org/10.1136/rapm-2020-101883>
 33. Park E, Chung SW (2019) ROS-mediated autophagy increases intracellular iron levels and ferroptosis by ferritin and transferrin receptor regulation. *Cell Death Dis* 10(11):822. <https://doi.org/10.1038/s41419-019-2064-5>
 34. Krause A, Neitz S, Mägart HJ, Schulz A, Forssmann WG, Schulz-Knappe P, Adermann K (2000) LEAP-1, a novel highly disulfide-bonded human peptide, exhibits antimicrobial activity. *FEBS Lett* 480(2-3):147–150. [https://doi.org/10.1016/s0014-5793\(00\)01920-7](https://doi.org/10.1016/s0014-5793(00)01920-7)
 35. Park CH, Valore EV, Waring AJ, Ganz T (2001) Hepcidin, a urinary antimicrobial peptide synthesized in the liver. *J Biol Chem* 276(11):7806–7810. <https://doi.org/10.1074/jbc.M008922200>
 36. Raha AA, Vaishnav RA, Friedland RP, Bomford A, Raha-Chowdhury R (2013) The systemic iron-regulatory proteins hepcidin and ferroportin are reduced in the brain in Alzheimer's disease. *Acta Neuropathologica Commun* 1:55. <https://doi.org/10.1186/2051-5960-1-55>
 37. Derry PJ, Hegde ML, Jackson GR, Kaye R, Tour JM, Tsai AL, Kent TA (2020) Revisiting the intersection of amyloid, pathologically modified tau and iron in Alzheimer's disease from a ferroptosis perspective. *Prog Neurobiol* 184:101716. <https://doi.org/10.1016/j.pneurobio.2019.101716>
 38. Blomster LV, Cowin GJ, Kurniawan ND, Ruitenberg MJ (2013) Detection of endogenous iron deposits in the injured mouse spinal cord through high-resolution ex vivo and in vivo MRI. *NMR Biomed* 26(2):141–150. <https://doi.org/10.1002/nbm.2829>
 39. Urrutia PJ, Hirsch EC, González-Billault C, Núñez MT (2017) Hepcidin attenuates amyloid beta-induced inflammatory and pro-oxidant responses in astrocytes and microglia. *J Neurochem* 142(1):140–152. <https://doi.org/10.1111/jnc.14005>
 40. Li JZ, Fan BY, Sun T, Wang XX, Li JJ, Zhang JP, Gu GJ, Shen YJ, et al (2023) Bioinformatics analysis of ferroptosis in spinal cord injury. *Neural Regen Res* 18(3):626–633. <https://doi.org/10.4103/1673-5374.350209>
 41. Wang F, Li J, Zhao Y, Guo D, Liu D, Chang S, Qiao H, Li J, et al (2022) miR-672-3p promotes functional recovery in rats with contusive spinal cord injury by inhibiting ferroptosis suppressor protein 1. *Oxidative Med Cell Longev* 2022:6041612. <https://doi.org/10.1155/2022/6041612>
 42. Shao C, Chen Y, Yang T, Zhao H, Li D (2022) Mesenchymal stem cell derived exosomes suppress neuronal cell ferroptosis via lncGm36569/miR-5627-5p/FSP1 axis in acute spinal cord injury. *Stem Cell Rev Rep* 18(3):1127–1142. <https://doi.org/10.1007/s12015-022-10327-x>

Publisher's Note Springer Nature remains neutral with regard to jurisdictional claims in published maps and institutional affiliations.

Springer Nature or its licensor (e.g. a society or other partner) holds exclusive rights to this article under a publishing agreement with the author(s) or other rightsholder(s); author self-archiving of the accepted manuscript version of this article is solely governed by the terms of such publishing agreement and applicable law.